

Cold Season Synoptic-Scale Waves over Subtropical South America

CAROLINA S. VERA

CIMA/Departamento de Ciencias de la Atmósfera, Universidad de Buenos Aires–CONICET, Buenos Aires, Argentina

PAULA K. VIGLIAROLO

CADIC–CONICET, Ushuaia, Argentina

ERNESTO HUGO BERBERY

Department of Meteorology, University of Maryland, College Park, College Park, Maryland

(Manuscript received 15 December 2000, in final form 5 July 2001)

ABSTRACT

The most active winter synoptic-scale wave patterns over South America are identified using an extended empirical orthogonal function (EOF) technique and are physically diagnosed using composite methods. Results show that the leading modes of short timescale variability propagate along two main paths: over the subtropical jet latitudes ($\sim 30^\circ\text{S}$) and over the subpolar jet latitudes ($\sim 60^\circ\text{S}$). This research focuses on the subtropical mode and its evolution over South America.

The observed structure of the systems associated with the subtropical mode resembles that of midlatitude baroclinic waves. Both cyclonic and anticyclonic perturbations display significant modifications in their three-dimensional structure as they evolve over extratropical and subtropical South America. While the upper-level perturbations are mostly unaffected when moving eastward, the lower-level perturbations advance following the shape of the Andes Mountains and exhibit an abrupt equatorward migration at the lee side of the mountains. As a result of such detachment, smaller eddy heat fluxes are observed in the vicinity of the orography and consequently a weaker eddy baroclinic growth is observed. Once the upper-level system is on the lee side, the perturbations acquire a more typical baroclinic wave structure and low-level intensification of the system occurs. The latter is largest around 1000 km east of the orography, where enhanced moisture transports from tropical latitudes along the eastern portion of the low-level cyclone favor precipitation occurrence over southeastern South America. Those precipitation processes seem to provide a diabatic source of energy that further contributes to the strengthening of the low-level cyclone. In addition, an intensification of the cyclone once over the ocean was found in 60% of the situations considered, which is consistent with previous research suggesting an additional source of moisture and heat flux due to the warm waters of the Brazil Current.

1. Introduction

The Southern Hemisphere (SH) storm track has been known for its predominant zonality and smooth longitudinal changes, as is the case of the geopotential height standard deviation that does not vary by more than 50% along the band between 40° and 60°S (Trenberth 1981). Still, Berbery and Vera (1996) presented evidence that the character of the transients is region dependent, a fact attributed to changes in the basic state. In the vicinity of South America, upper-level waves acquire a NW–SE horizontal orientation while progressing to the northeast, departing from the general concept of zonality (Berbery and Vera 1996; Chang 1999).

The most relevant feature of South America's topog-

raphy is the Andes Cordillera along the western part of the continent, from the Tropics to about 55°S . Around 20°S there is a high-level plateau (known as the Altiplano) with a mean elevation of around 3800 m and 300 km wide. Except over this area, where the orientation is northwest–southeast, the mountains have a north–south orientation. From the Altiplano to about 35°S they are about 3000 m high, decaying farther south to about 1500 m and a cross section of around 300 km.

According to Gan and Rao (1994) transient disturbances of geopotential height approaching the Andes exhibit a zonal trajectory at upper levels. But at lower levels, perturbation centers experience an anticyclonic turning while they elongate equatorward on the lee side of the orography. As a consequence, the vertical tilt of the systems increases as they cross the mountains. Gan and Rao (1994) suggest that this must result in baroclinic development as predicted from the linear normal-mode

Corresponding author address: Dr. Carolina S. Vera, CIMA, Pab. 2, 2do Piso, Ciudad Universitaria, 1428 Buenos Aires, Argentina.
E-mail: carolina@at.fcen.uba.ar

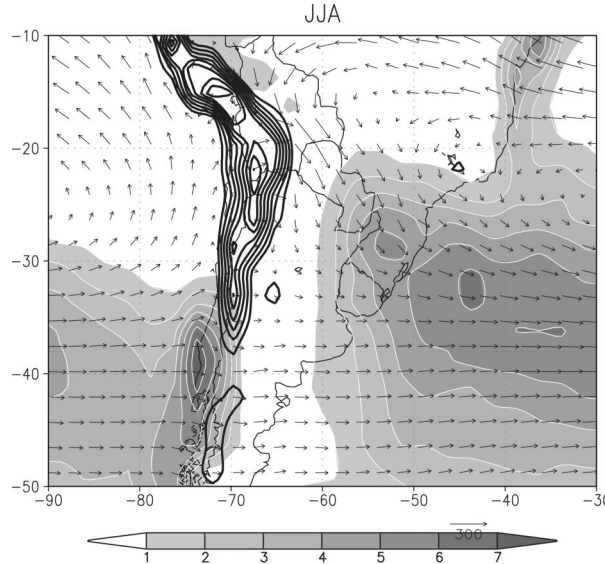


FIG. 1. Mean total precipitation (from Xie and Arkin 1997) and vertically integrated moisture fluxes (from ERA-15) averaged from Jun through Aug 1979–93. Contour interval is 1 mm day^{-1} . Vector units are $\text{kg} (\text{m s})^{-1}$. Orography higher than 1000 m is contoured in black.

theory in the presence of mountains (Buzzi and Tosi 1989).

Midlatitude disturbances such as intense cold fronts and cutoff lows are a very important cause of severe weather events over the southern part of South America, mainly during austral winter. In particular, upper-level cold cyclones propagate eastward from the Pacific Ocean at around 30°S and intensify near the surface over southeastern South America producing significant rainfall. Taljaard (1972), Necco (1982a,b), Gan and Rao (1991) and recently Simmonds and Keay (2000) have documented that cyclogenesis is rarely found between the Andes and 60°W , while the eastern part of the continent and the adjacent Atlantic Ocean, between 20°S and 35°S , is a preferred region of cyclogenesis occurrence, with a maximum of precipitation over that same area (Fig. 1).

The most productive areas of Argentina, Uruguay, and Brazil, in terms of agriculture and hydroelectric power generation, are highly affected by cyclogenesis. Large NW–SE mean moisture fluxes east of the Andes Mountains transport moisture from tropical latitudes into the subtropics (see, e.g., Berbery and Collini 2000) and there are indications that this occurs regardless of the season; these fluxes may be relevant for the development of the cyclones. The evolution of these systems has been mainly explored through extreme-case studies using observations (Jusem and Atlas 1991) or numerical model simulations (Seluchi and Saulo 1998, among others). But there is a lack of statistical studies that describe the mean dynamical characteristics of such cyclones and their contribution to winter precipitation.

Anticyclogenesis is usually found behind advancing

cold fronts at the lee side of the Andes. Poleward of 38°S (where the Andes are lower) cold air masses move around the mountains with enhanced divergence and subsidence. The orography acts like a dam on the easterly flow associated with the anticyclonic anomaly, resulting in anticyclogenesis over central Argentina (see, e.g., Vera and Vigliarolo 2000). The associated cold air surges that may produce freezing conditions from central Argentina to southern Brazil have been extensively studied in several papers (see Garreaud 2000 and references therein). However, the changes in the three-dimensional structure of the anticyclonic perturbations as they pass over South America are not well understood yet, and need further investigation.

The objective of this paper is to provide a large-scale diagnosis of the systems that evolve along subtropical South America during the austral winter. Particular attention is paid to the evolution of upper-level cyclonic perturbations and their role in facilitating precipitation over southeastern South America. The paper is organized as follows. The datasets and analysis procedure are described in section 2. Section 3 inspects the spatial features and temporal evolution of cyclonic perturbations that cross the Andes during austral winter at subtropical latitudes, while section 4 diagnoses the evolution of anticyclonic perturbations. A summary and final comments are presented in section 5.

2. Analysis technique

a. Data

The dataset consists of 15 austral winters (June–August 1979–93) of European Centre for Medium-Range Weather Forecasts (ECMWF) daily 1200 UTC reanalyses (known as ERA-15) with a $2^\circ \times 2^\circ$ grid resolution and 10 vertical levels. Daily averages of the National Oceanic and Atmospheric Administration (NOAA) satellite outgoing longwave radiation (OLR) field are used as a precipitation proxy, while daily precipitation observations at rain gauge stations in Argentina were also employed (see Fig. 6). Short time-scale perturbations are identified using the 300-hPa meridional wind perturbations (v') (Trenberth 1981; Chang 1993; Berbery and Vera 1996), obtained as the difference between each individual value and the time mean for the season, effectively removing the interannual variability from the series. No further filtering of the series was performed, since there is evidence that meridional wind variability is concentrated in the higher frequencies, a fact that is more so in the SH (Trenberth 1981; Hoskins et al. 1983).

b. Extended empirical orthogonal function analysis

An extended empirical orthogonal function (EEOF) analysis for four 1-day lag units was performed over a domain that extends from 130° to 20°W and from 80° to 10°S , to examine the structure and temporal evolution

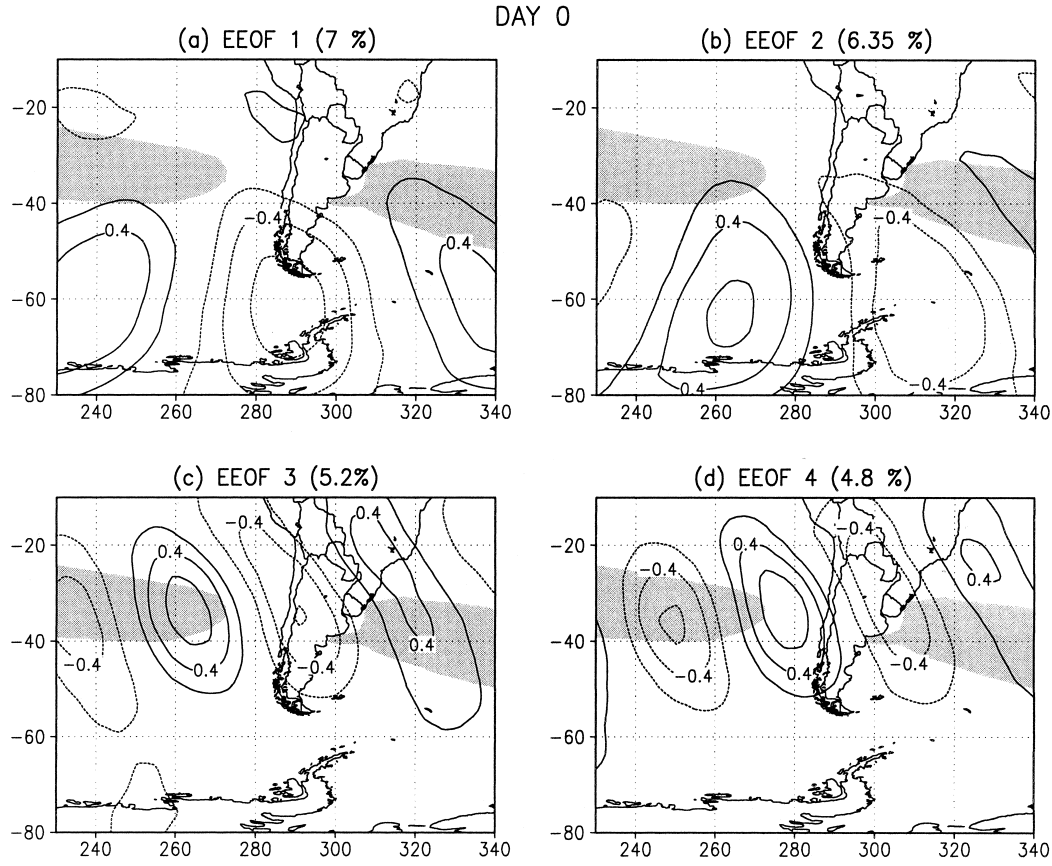


FIG. 2. (a)–(d) Factor loadings for the four leading EEOFs of meridional wind perturbation at 300 hPa over the South America domain at day 0. Contour interval is 0.2 and zero contour is omitted. The 300-hPa zonal mean wind values greater than 28 m s^{-1} are shaded.

of synoptic-scale waves over South America during austral winter. Numerous tests show that the leading modes do not depend on the size of the domain where the EEOF analysis is performed. It is assumed that a 5-day period is long enough to capture the evolution of baroclinic waves over the SH (Berberry and Vera 1996). The extended empirical orthogonal function technique (Weare and Nasstrom 1982) includes the temporal structure in the basic observation vectors; then, successive spatial patterns can describe the spatial structure and temporal evolution of the dominant modes. The EEOF modes were computed from the correlation matrix of the meridional wind perturbation temporal series at 300 hPa. For that reason, the resulting EEOF patterns best represent upper-level systems. However, tests indicate that the level where the analysis is performed is not critical for identifying the leading patterns. For example, a similar EEOF analysis on the 850-hPa meridional wind perturbation series (Vera and Vigliarolo 2000) produced two pairs of leading modes with similar characteristics to the ones shown here.

The first four EEOFs explain 7%, 6.35%, 5.2%, and 4.8%, respectively, of the total variance. According to Lau and Chan (1985) the fractional variance calculated

from an EEOF analysis performed using four lags is approximately one-fourth of that obtained from a conventional EOF analysis; thus, for all practical purposes these percentages are considered large. The four leading EEOFs have the typical horizontal structure of baroclinic waves; they appear in pairs that have a quadrature phase shift, representing the propagation of the same local wave (Fig. 2). This is a common characteristic of propagating disturbances such as synoptic-scale waves (e.g., Lau and Lau 1990). The first pair of modes (Figs. 2a,b) is associated with a wave train propagating along the subpolar jet, while the second pair (Figs. 2c,d) corresponds to a wave train evolving along the subtropical jet that crosses the Andes around 30°S .

The first mode was studied by Vigliarolo et al. (2001) in reference to its role in producing ozone variations and thus will not be addressed here. As stated earlier, modes 3 and 4 represent different phases of the same wave; here, the EEOF 4 mode (hereafter referred as subtropical mode) will be analyzed, as it is the one that better describes the perturbations maximizing in the vicinity of subtropical South America. To this end, composite maps of several meteorological variables were prepared to document the mode's three-dimensional

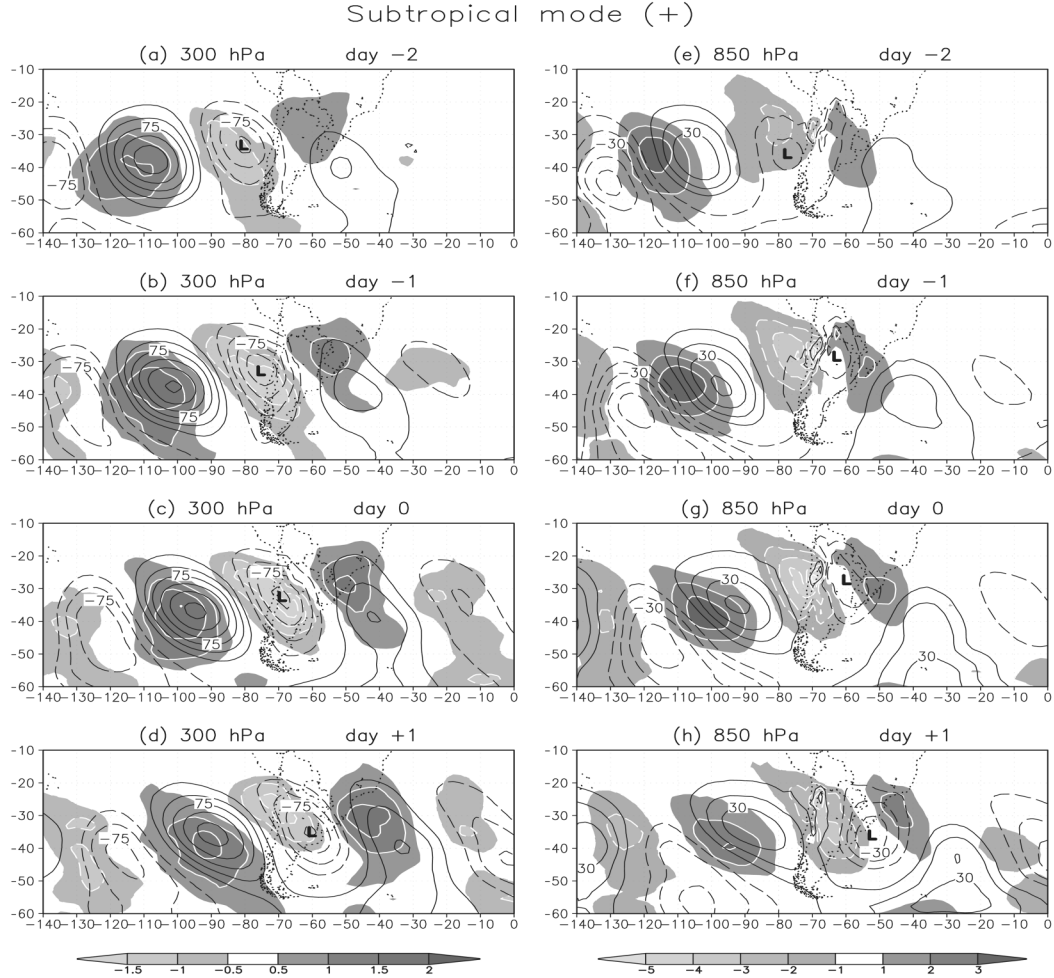


FIG. 3. (a)–(d) Positive composites for the subtropical mode of geopotential height perturbations and temperature perturbations at 300 hPa from day -1 to day $+2$. Contour interval is 20 m and shading interval is 0.5°C . (e)–(h) As in (a)–(d) but at 850 hPa. Contour interval is 10 m and shading interval is 1°C . Negative contours are dashed and zero contour is omitted. The L denotes the cyclone perturbation location under study.

structure and propagation characteristics. A positive (negative) composite field refers to the average of the meteorological situations that occurred when the values of the EEOF temporal coefficients are larger (smaller) than 1 (-1) times the standard deviation of the series. The statistical significance at the 5% level of all the composite fields was checked using a t test (not shown).

3. Cyclonic case

Positive temporal coefficients of the subtropical mode are associated with the passage of upper-level cyclonic perturbations over the Andes, while negative values correspond to anticyclonic perturbations (Fig. 2d). Several papers have shown that the synoptic-scale wavelike features identified through EEOF/EOF analyses like the one presented here are not merely mathematical artifacts and that they are closely related to real cyclonic and anticyclonic situations. For example, Lau and Lau

(1990) showed that patterns obtained from EEOF analyses depict well the characteristics of synoptic-scale waves at tropical latitudes. In particular Compagnucci and Salles (1997) found over extratropical South America a clear correspondence between the surface pressure maps resulting from a principal component analysis and the synoptic maps analyzed by the Argentine Meteorological Service.

Ninety-four situations associated with temporal coefficients larger than one standard deviation were identified and used to build the composite fields. In this section we will refer to it as the “positive composite.”

a. Horizontal wave structure

Positive composite fields of the 300- and 850-hPa geopotential height and temperature perturbations from day -2 to day $+1$ associated with the subtropical mode are presented in Fig. 3. The temporal evolution of the

upper-level waves (Figs. 3a–d) shows that over the southeastern Pacific Ocean waves propagate equatorward, as expected from the simulations of Yu and Hartmann (1995) for waves with similar periods in the vicinity of orography [the period for subtropical waves, as estimated in Berbery and Vera (1996), is typically 7–8 days]. Upper-level perturbations (Figs. 3a–d) also exhibit the typical baroclinic wave pattern of warm highs and cold lows with temperature perturbation centers to the southwest of the geopotential height ones [consistent with Chang's (1993) results for the Northern Hemisphere (NH)]. However, on the lee side of the Andes, upper-level temperature perturbations are found to the northwest of the height centers (Fig. 3d), suggesting changes in the thermal structure of the waves as they cross the Andes.

Between days -2 and -1 , the upper-level cyclone intensifies to a maximum west of the topography (Figs. 3a,b), as in Yu and Hartmann's (1995) simulations. At day 0, it maintains its strength (Fig. 3c) while during the following days it begins to decay on the lee side at around 35°S (Fig. 3d).

Also between days -2 and -1 , the cyclone at lower levels goes around the Andes between 35° and 40°S and then experiences a fast equatorward movement (Figs. 3e,f), in agreement with Gan and Rao (1994) and Seluchi et al. (1998). At day 0 (Fig. 3g) the cyclone, at around 30°S , 60°W , becomes more localized. Similar wave changes have been detected in the vicinity of the Rockies and explained as evidences of topographic Rossby waves that tend to conform to the shape of the terrain with a spatial scale comparable to that of the topography (Hsu and Wallace 1985; Hsu 1987; Buzzi and Tosi 1989, among others). Furthermore, Davis (1997) showed that the behavior of those waves is actually controlled by the gradients of surface potential temperature modified by the orography. By day $+1$ (Fig. 3h) composites show that the cyclone moves southeastward and intensifies over the eastern coast of Uruguay and Argentina, more than 1000 km away from the orography.

The evolution depicted in Fig. 3 essentially resembles the progress of upper-level cold troughs that during austral winter move eastward from the South Pacific Ocean to subtropical South America and that may develop in cyclogenesis events over the eastern coast of the continent (Necco 1982a,b). These types of situations are frequent in the region and they have only been analyzed through the study of individual cases. Seluchi and Saulo (1998) explored the mechanisms yielding an explosive coastal cyclogenesis over South America using a limited area model. In their Fig. 1 they present the corresponding evolution of the geopotential heights at middle and low levels, which is very similar to the one presented in our Fig. 3. Also, Jusem and Atlas (1991) made a diagnosis of another case that occurred in May 1984 with rapid cyclogenesis off the eastern South American coast. In particular, they present a detailed synoptic overview of

that particular case using both ECMWF (their Figs. 3–6) and manual analyses (their Figs. 7 and 8) that also has a significant parallelism with the evolution described by the positive composites fields (Fig. 3).

b. Vertical wave structure

Longitude–height sections averaged between 35° and 25°S of meridional wind, geopotential height, and temperature perturbations and eddy meridional heat fluxes are presented in Fig. 4 for day -1 , which is when the low-level cyclone tracks around the orography. Both meridional wind and geopotential height perturbations (Figs. 4a,b) present a vertical structure that maximizes at upper levels, as is typical for synoptic-scale waves (Lim and Wallace 1991; Chang 1993 for the NH). In addition, the perturbation maximum is found higher toward the east, suggesting upward energy dispersion. Also, by that time the vertical tilt of the cyclone becomes too large and its low-level portion on the lee side is out of phase from its counterpart above, which is still located over the Pacific Ocean (Fig. 4b). Several papers (e.g., Blackmon et al. 1979) have already documented that as weather systems move across mountain ranges, the vertical structure of atmospheric patterns undergoes a transition from equivalent barotropic to more baroclinic; it is also likely that the low-level circulation pattern may become partially detached from the corresponding upper-level wave as suggested by Hsu (1987). During the following days, as the upper-level trough moves eastward, the difference in phase between upper- and lower-level perturbations decreases (figures not shown).

The vertical structure of the temperature perturbations also exhibits significant modifications in the vicinity of the orography (Fig. 4c). Temperature perturbations over the Pacific Ocean maximize at the lower troposphere between 500 and 700 hPa with a sign reversal around 250 hPa, like baroclinic waves do over the North Pacific Ocean (Lim and Wallace 1991; Chang 1993). However, on the lee side of the Andes, the warm center has a maximum at around 800 hPa, a sign reversal located farther up, and a significantly weaker stratospheric maximum.

c. Precipitation and moisture fields

Composite fields of OLR perturbations associated with the positive values of the subtropical mode (cyclonic) from day -1 to day $+1$ are presented in Fig. 5. At day -2 (not shown) negative OLR anomalies representing positive anomalies of precipitation are found to be associated with the passage of the low-level cyclone over the Andes between 30° and 40°S (Fig. 3e). By day -1 (Fig. 5a) the OLR anomalies extend over central and northern Argentina while at day 0 the precipitation area spreads over southern Bolivia, Paraguay, and eastern Argentina, with a con-

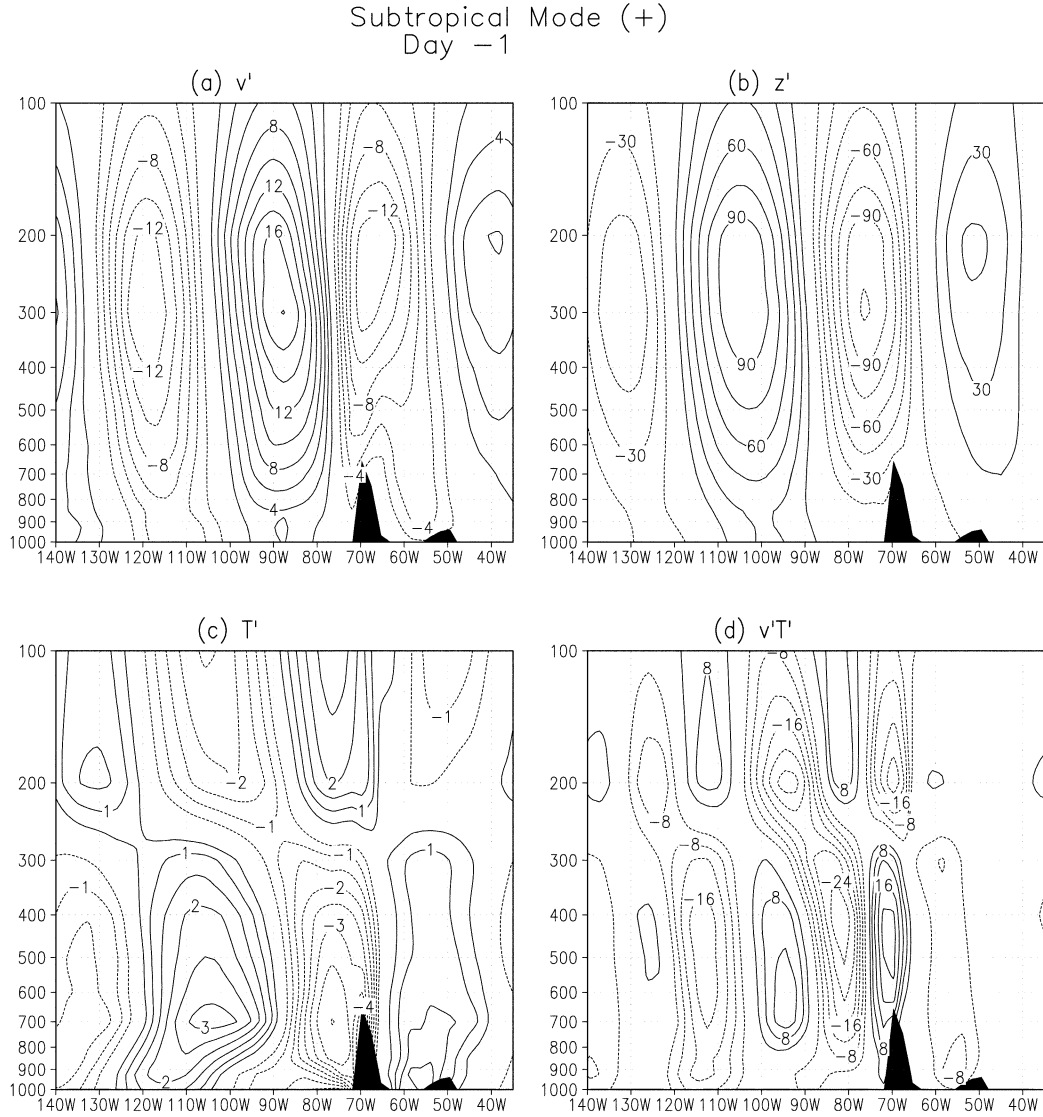


FIG. 4. Longitude-height cross section of positive composites for the subtropical mode of (a) meridional wind perturbations, (b) geopotential height perturbations, (c) temperature perturbations, and (d) eddy meridional heat fluxes, averaged between 35° and 25° S at day -1 . Contour intervals are (a) 2 m s^{-1} , (b) 15 m , (c) 0.5°C , and (d) $4 \text{ m s}^{-1}^{\circ}\text{C}$. Negative contours are dashed and zero contour is omitted. A sketch of the orography is included for reference.

spicuous maximum over southern Brazil and Uruguay (Fig. 5b). By day $+1$, the band of negative OLR anomalies has moved northeastward without losing intensity and acquired an elongated structure in the NW–SE direction (Fig. 5c).

Composite fields of precipitation were prepared using daily rainfall data available from surface stations over Argentina. For each particular station and lag time, precipitation occurring during days associated with positive temporal coefficients (larger than one standard deviation) was accumulated over each individual winter. Then, the accumulated precipitation values were normalized by the total accumulated precipitation of that particular winter, and finally averaged over all years.

The resulting quantity, multiplied by 100, represents the percentage of winter mean accumulated precipitation explained by the subtropical mode. Figure 6 shows that the precipitation accumulated over all the cyclonic situations lasting 5 days associated with the subtropical mode explains more than 60% of the mean winter accumulated precipitation over central and northeastern Argentina for that particular period. This result certainly reflects the importance of these synoptic phenomena on accounting for winter total precipitation over southeastern South America. The remaining 40% is the result of weaker systems (recall that composites are constructed only by those cases where the temporal component of the EEOF is larger than 1 times the standard devi-

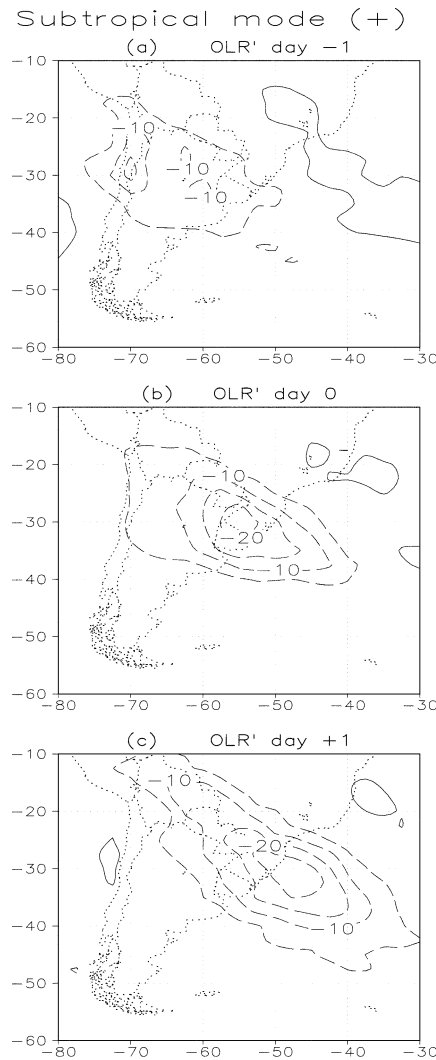


FIG. 5. (a)–(c) Positive composites for subtropical mode of OLR' perturbations from day -1 to day $+1$. Contour interval is 5 W m^{-2} , negative contours are dashed, and zero contour is omitted.

ation) and other frontal systems associated with EEOFs 1 and 2 (Figs. 2a,b).

An analysis of atmospheric water vapor content (precipitable water) and water vapor flux fields contributes to a better understanding of the precipitation processes previously described. The left panels of Fig. 7 depict the evolution of vertically integrated moisture fluxes by the perturbations and the associated divergence field, while the precipitable water anomalies are shown in the right panels.

Figure 7a shows that eastward of the cyclonic perturbation on day -1 (Fig. 3f) there are enhanced poleward moisture fluxes transporting moisture from tropical to middle latitudes near 60°W . The precipitable water anomalies (Fig. 7d) exhibit a band of large values also along 60°W with a maximum at around 25°S . At day 0 (Fig. 7e), they attain their maximum value over eastern

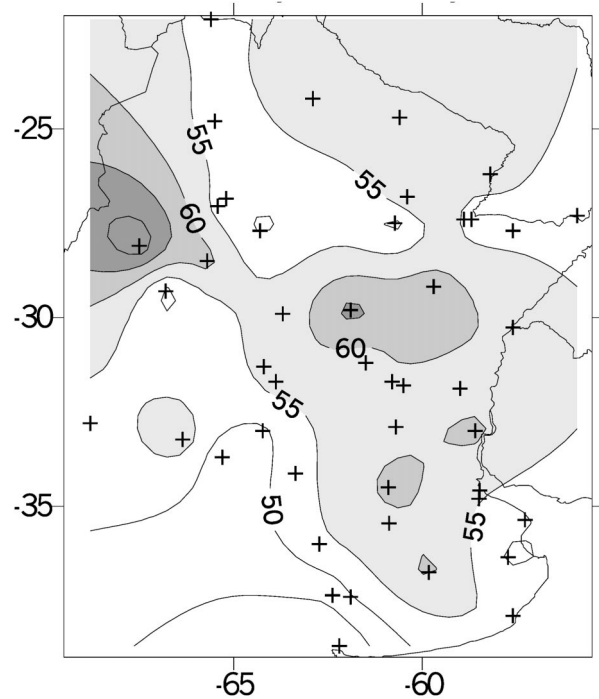


FIG. 6. Percentage ($\times 100$) of winter mean accumulated precipitation from day -2 to day $+2$ explained by the positive phase of the subtropical mode. Contour interval is 5% and values larger than 55% are shaded. Crosses indicate distribution of Argentinean rain gauges.

Argentina and southern Brazil. Moisture fluxes have a NW–SE direction presenting the largest convergence over Uruguay (Fig. 7b). One day later, moisture fluxes are still strong, converging over the Atlantic Ocean (Fig. 7c), while precipitable water decays markedly along a band with a pronounced NW–SE orientation and largest values over the coast.

Longitude–height sections of meridional moisture transports by the perturbations and moisture anomalies averaged between 35° and 25°S are presented in Fig. 8. At day -1 , both fields exhibit significant values in the 1000–400-hPa layer, their vertical structures are slightly tilted westward, and both maximize at around 850 hPa (Figs. 8a,d). At day 0, poleward moisture fluxes are most intense and their largest values are found between 850 and 700 hPa (Fig. 8b). Moreover, moisture perturbations also are largest at 850 hPa while they exhibit a wider longitudinal section (Fig. 8e). By day $+1$, both fields decay, and meridional moisture fluxes have their maximum at around 600 hPa while a secondary maximum is also observed at surface between 50° and 40°W (Fig. 8c). Moisture anomalies also show a secondary maximum near the ground while maintaining their maximum values at around 850 hPa. As will be discussed in the next section, the secondary moisture maximum is located over the warm waters of the Brazil Current, suggesting an additional source of moisture from the ocean.

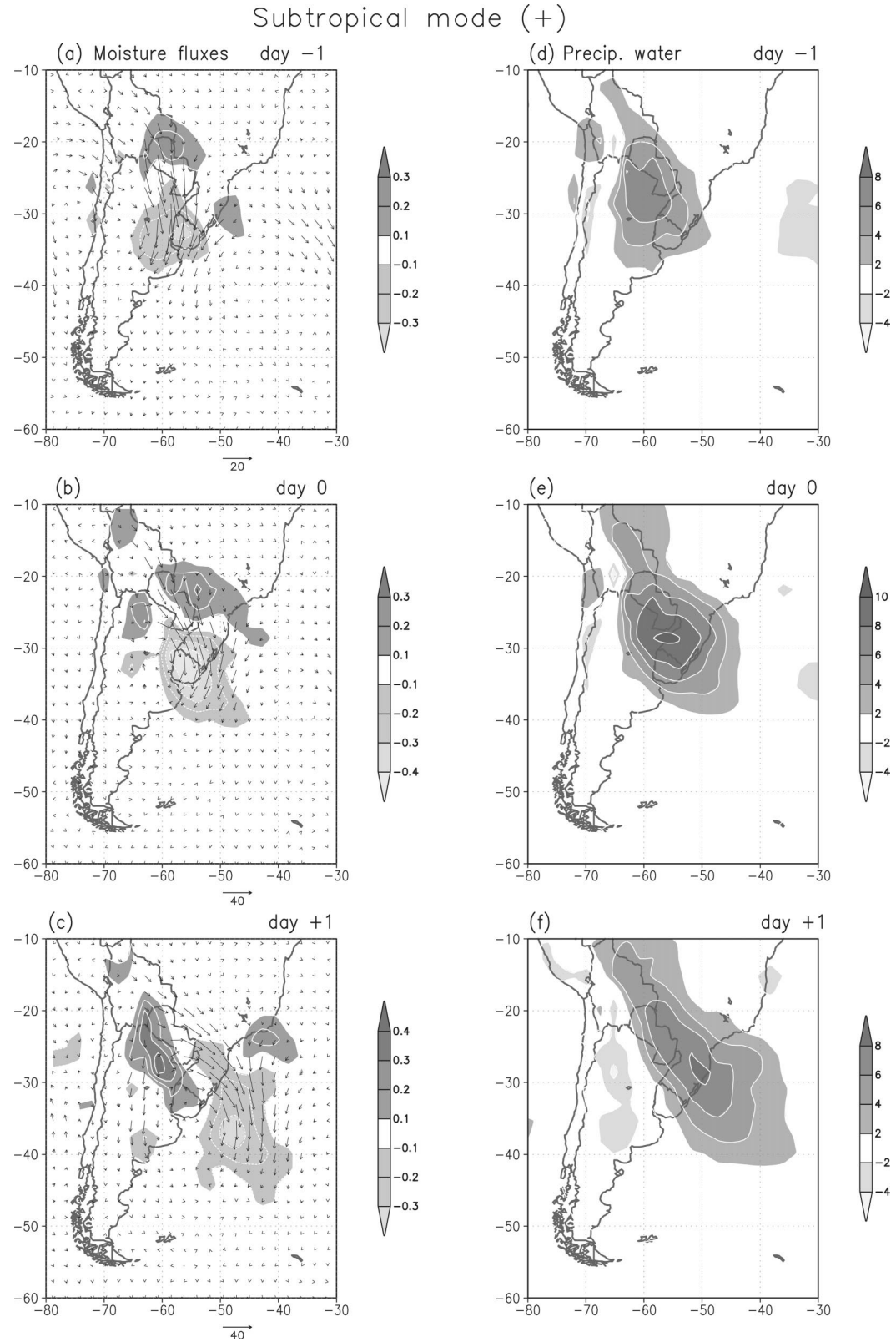


FIG. 7. (a)–(c) Positive composites for the subtropical mode of both vertically integrated moisture fluxes (vectors) and moisture flux divergence (contours) by the perturbations from day -1 to day $+1$. Contour interval is $1 \times 10^5 \text{ kg m}^{-2} \text{ s}^{-1}$ and vector units are kg (m s)^{-1} . (d)–(f) As in (a)–(c) but for precipitable water perturbation. Contour interval is 2 mm. Negative contours are dashed and zero contour is omitted.

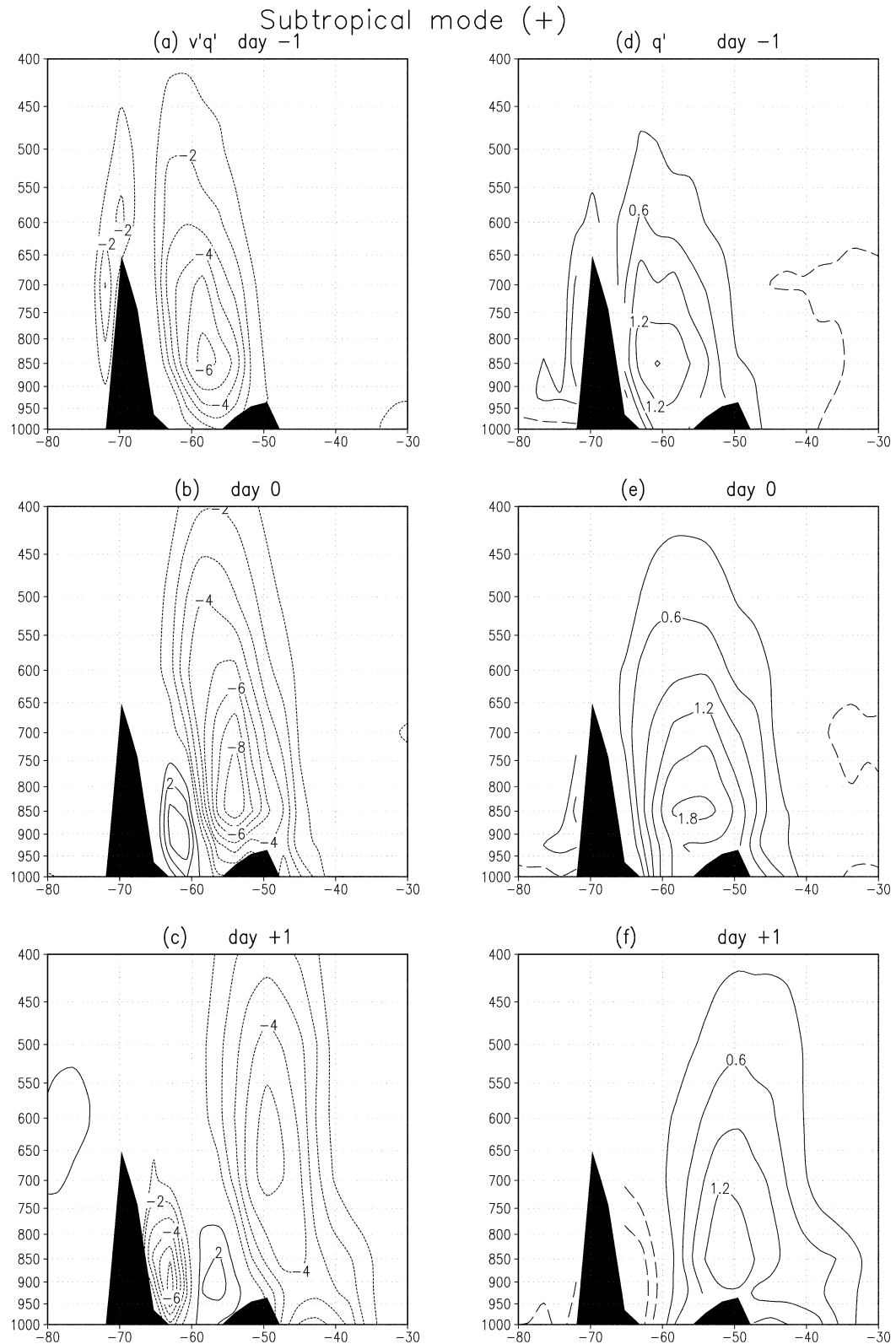
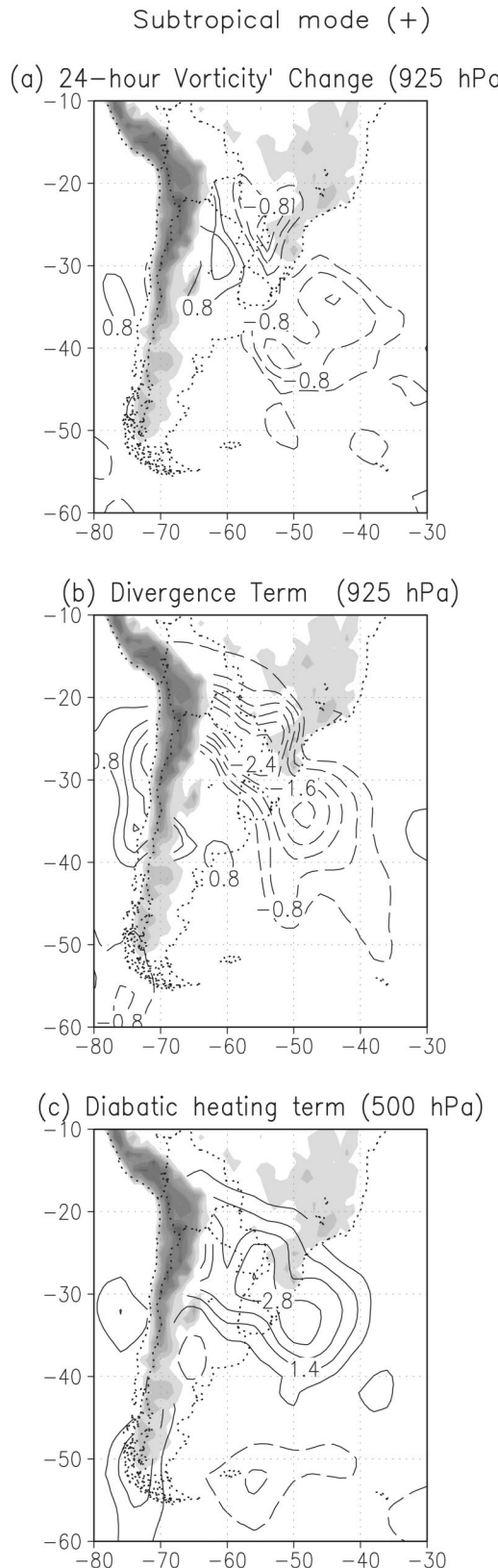


FIG. 8. Longitude-height cross section of positive composites from day -1 to day +1 for the subtropical mode of (a)–(c) moisture fluxes by the perturbations and (d)–(f) specific humidity perturbations, averaged between 35° and 25° S. Contour interval is (a)–(c) $1 \text{ g kg}^{-1} \text{ m s}^{-1}$ and (d)–(f) 0.3 g kg^{-1} . Negative contours are dashed and zero contour is omitted. A sketch of the orography is included for reference.



d. Low-level cyclone intensification

Uccellini (1990) provides an excellent review of the possible factors contributing to the development of cyclonic systems and the critical processes that favor rapid cyclogenesis. He found that there is a great consensus that 1) superimposed upper- and lower-tropospheric dynamic processes are required for cyclogenesis and 2) development rates are significantly enhanced by the interaction of diabatic and dynamic processes, especially those that are related to the release of latent heat and those that act to reduce the static and symmetric stability of the lower troposphere. Regarding factor 1, changes to the baroclinic wave vertical structure due to the presence of the Andes, previously described in section 3b, have a strong impact on the vertical distribution of eddy meridional heat fluxes and, thus, on the wave's baroclinic growth (Berberry and Nuñez 1987).

According to Fig. 4d, meridional eddy heat fluxes over the Pacific Ocean at day -1 maximize at around 500 hPa and, with reversed sign, at around 200 hPa; as expected, poleward heat fluxes are the strongest. On the other hand, equatorward fluxes are intense just to the west of the Andes while very weak poleward fluxes are observed on the lee side with a maximum at around 800 hPa. Two days later the cyclonic perturbation over the continent turns to a more classical baroclinic wave structure with eddy heat fluxes becoming more intense (not shown) and the low-level cyclone intensifying (Fig. 3h).

An analysis of local changes of perturbation vorticity at 925 hPa (Vera and Vigliarolo 2000) shows that the divergence term $-(\bar{s} + f)\nabla \cdot \mathbf{v}'$ [VD_e from their Eq. (1)] is the main factor in low-level cyclonic-vorticity development over southeastern South America between day 0 and day +1 (Figs. 9a,b). The enhancement of the low-level convergence is associated with an increment of ascending motion at middle levels (not shown). Through an analysis of the thermodynamic equation at 500 hPa, it was found that the latent heat released (Fig. 9c) by the precipitation events is the main contributor to enhance upward vertical motion east of the cyclone. Seluchi and Saulo (1998) through numerical simulations of a case study have also identified this process as a key factor in the rapid cyclogenesis over southeastern South America.

Between day 0 and day +1, the 1000-hPa geopotential height perturbation center drops as the system moves off the coast into the ocean (Figs. 10a,b) and it continues falling through day +2 (not shown). During that 3-day



FIG. 9. Positive composites for subtropical mode of (a) 24-h vorticity perturbation change and (b) divergence term. Both terms are from the relative vorticity equation at 925 hPa and at day 0. Contour interval is $0.4 \text{ s}^{-1} \text{ day}^{-1}$. (c) Diabatic heating term from the thermodynamic equation at 500 hPa and at day 0. Contour interval is 0.7 K day^{-1} . Negative contours are dashed and zero contour is omitted. Orography higher than 1000 m is shaded.

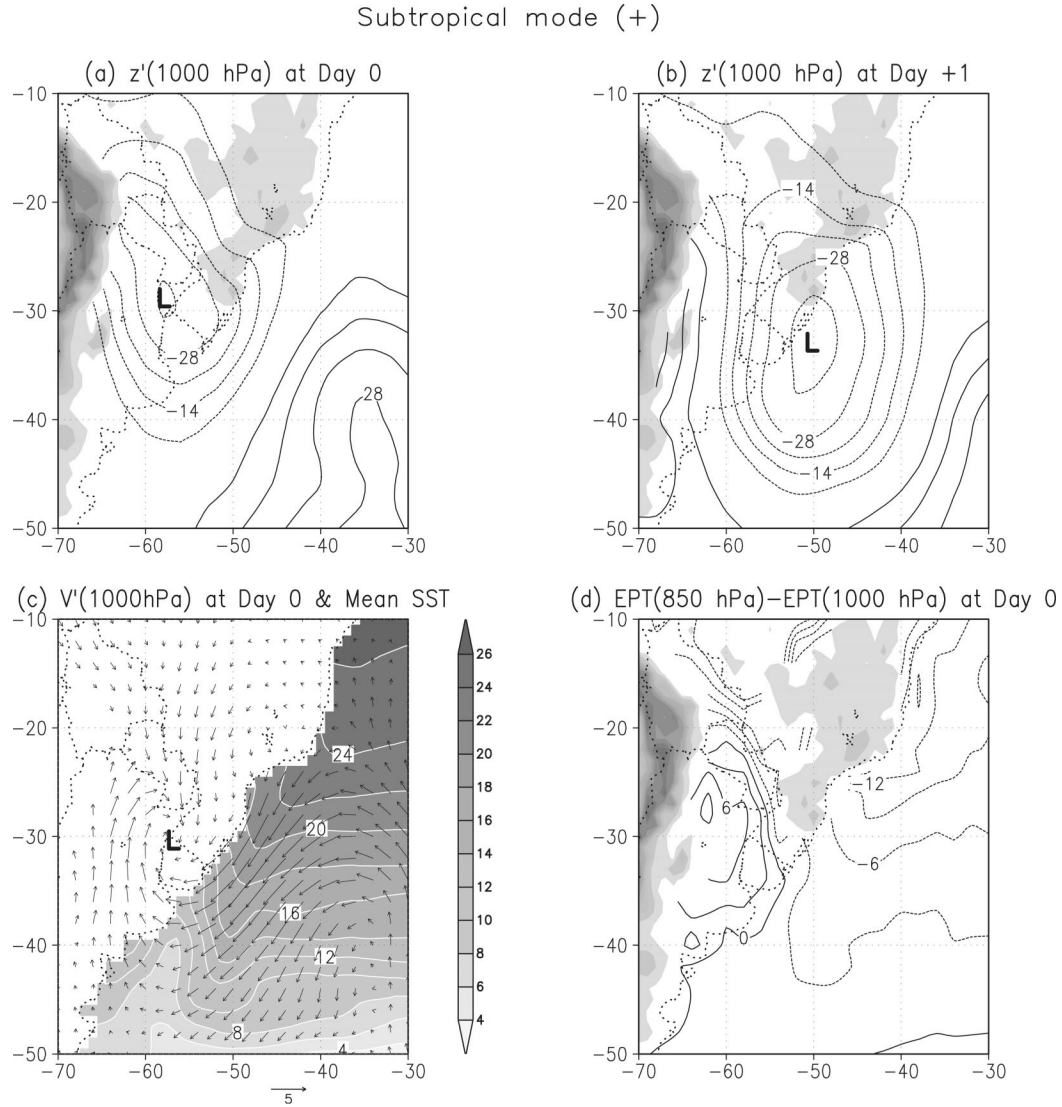


FIG. 10. Positive composites for the subtropical mode of 1000-hPa geopotential height at (a) day 0 and (b) day +1. Contour interval is 7 m and zero contour is omitted. (c) Positive composites of 1000-hPa wind perturbations (vector units in 1 m s^{-1}) at day 0 and winter mean sea surface temperatures contoured every 2°C (shaded). (d) Positive composites of equivalent potential temperature differences between 850 and 1000 hPa at day 0 contoured each 3 K. Orography higher than 1000 m is shaded in (a), (b), and (d). The L denotes the cyclone perturbation location under study.

period, the cyclonic perturbation center value at 1000 hPa goes from -35 m over land at day 0, to -40 m at day +1 and to -50 m by day +2. Due to the fact that these values are the result of a composite based on upper-level meridional wind perturbations, the drop in 1000-hPa heights is not that dramatic. However, inspection of individual cases within the composite showed more significant height drops; in one case (10 June 1992), the 1000-hPa geopotential height center deepened by about 240 m in 2 days. This is consistent with Seluchi and Saulo (1997) who showed that the 24-h drop of the 1000-hPa geopotential height center that

characterizes coastal cyclogenesis can range between -50 and -350 m .

It was also found that in 60% of the situations considered in the composites, as the systems move off South America there is cyclone reinforcement at the location displayed in Fig. 10b. On the other hand, in the rest of the situations, cyclone strengthening takes place over the continent (Fig. 10a). However, composites resemble the situations that characterize cyclone reinforcement over the sea because the minimum at the cyclone center in these situations is an average of 25% deeper and its corresponding 24-h drop is 50% larger than in those

cases where the cyclone strengthening occurs over land. These results were also confirmed independently from the EEOF analysis, quantifying all cases that occurred over the 15-winter period in which a surface cyclone moves off that particular region of South America toward the sea.

During winter, a strong land-sea contrast of equivalent potential temperature occurs over that coast equatorward of 35° , due to the presence of the poleward warm Brazil current (Peterson and Stramma 1991). It has been found that this region is cyclogenetic (Taljaard 1972; Necco 1982a) and a case study by Saraiva and Silva Dias (1997) suggests that local horizontal gradients of sea surface temperature (SST) have a strong influence on the trajectory and evolution of the surface cyclone. In the results presented here (Figs. 3e–h) the low-level temperature perturbations from day 0 to day +2 (Figs. 3e–h) show a warm center propagating equatorward along the coasts of Uruguay and southern Brazil, associated with the reinforcement of the low-level cyclonic perturbation. In particular by day 0, warm temperature advection achieves a maximum over the ocean where intense low-level wind perturbation flow parallel to the coast and along the warm Brazil Current is observed (Fig. 10c).

The effect of sensible and latent heat fluxes in the planetary boundary layer on rapid cyclogenesis off the southeastern coast of South America has received very little attention [Saraiva and Silva Dias (1997) is just one of the few studies available]. On the other hand, many studies have shown that similar cyclogenetic events frequently take place along the eastern coast of North America during the cold season: recent results show that, besides the latent heat release from precipitation processes, surface evaporation and surface sensible heat influx from the underlying warm water of the Gulf Stream are important contributors to cyclone development over that particular coast (Mak 1998; Carrera et al. 1999).

The exploration of the degree to which sensible and latent heat fluxes in the lower troposphere act to fuel cyclogenesis off the southeastern coast of South America is beyond the goal of this paper. However, it is not unlikely that these processes are similar to those off the coast of North America. They would act to decrease the low-level static stability in the cyclogenetic region. Static stability is an important factor in determining the secondary circulations of fronts and jets and controlling the baroclinic growth rates (Uccellini 1990). Walsh et al. (1988) showed that atmospheric sensible heating over the warm ocean surface decreases the moist-adiabatic lapse rate prior to and during rapid cyclogenesis over the North Pacific Ocean. Consistent with this, composites of equivalent potential temperature differences between 1000 and 850 hPa at day 0 (Fig. 10d) shows stable conditions over the continent south of 20°S while moist unstable conditions are observed away from the coast.

4. Anticyclonic case

Ninety-three situations associated with temporal coefficients of the subtropical mode less than -1 times the standard deviation were identified and used to build composite fields that correspond to the passage of anticyclonic perturbations over the Andes (for brevity, we will refer to this as the negative composite). Such perturbations, usually located behind surface fronts, force cold air from higher latitudes to penetrate equatorward to the east of the orography and may be associated with freezing events over extratropical and tropical South America (see, e.g., Marengo et al. 1997). The dynamical processes associated with cold surges were documented by Vera and Vigliarolo (2000) and Garreaud (2000); here, the interest is on the changes of the three-dimensional structure of the anticyclonic perturbation as it evolves over the Andes. Results are compared to those of the cyclonic perturbation.

Figure 11 presents the temporal evolution of the negative composite fields of 300- and 850-hPa geopotential height and temperature perturbations associated with the subtropical mode from day -2 to day 0. During the evolution, geopotential height perturbations at upper levels (Figs. 11a–c) exhibit an equatorward propagation that is more pronounced on the lee side of the Andes. From day -2 to day -1 (Figs. 11a,b), the upper-level ridge approaches the Andes, maximizing just west of the topography. Between day -1 and day 0 (Figs. 11b,c) the anticyclonic system crosses the Andes around 40°S with a strong NW–SE horizontal tilt while the cyclonic system ahead of it intensifies and progresses northeastward over the Atlantic Ocean.

Between day -2 and day -1 (Figs. 11d,e), the low-level anticyclone crosses the Andes farther south compared to the cyclone while it impels cold air equatorward into subtropical and tropical regions. It is evident that by day -1 the anticyclonic perturbation intensifies east of the topography, a characteristic not observed in the cyclonic case (Fig. 3). Vera and Vigliarolo (2000) have shown that the anticyclonic perturbation enhancement on the lee side is produced by the strong ageostrophic meridional circulation occurring on the poleward side of the surface front. By day 0, the anticyclone center is over eastern Argentina and begins to weaken (Fig. 11f).

A longitude-height section of the composite fields, averaged between 35° and 25°S , is depicted in Fig. 12. Most of the features for the anticyclonic case resemble those found for the cyclone such as a large westward tilt with the height of the meridional wind and geopotential height perturbations, the evidence of upward energy propagation (figures not shown), and weaker eddy heat fluxes occurring over the continent than over the ocean (Fig. 12b).

The vertical structure of the temperature perturbation associated with the anticyclone exhibits, over the continent, a cold air core with a maximum at 925 hPa and a strong eastward vertical tilt up to 600 hPa (Fig. 12a)

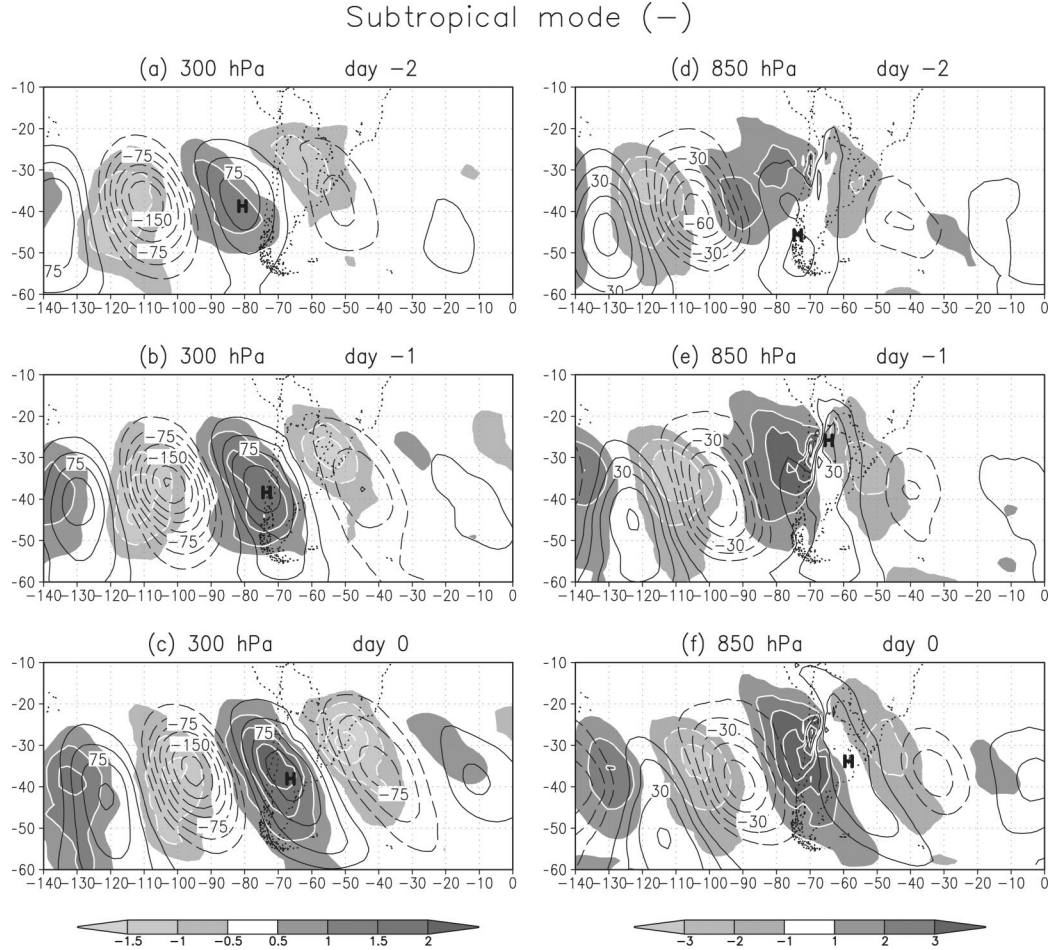


FIG. 11. (a)–(c) Negative composites for the subtropical mode of geopotential height perturbations and temperature perturbations at 300 hPa from day -1 to day $+1$. Contour interval is 20 m and shading interval is 0.5°C . (d)–(f) As in (a)–(c) but at 850 hPa. Contour interval is 10 m and shading interval is 1°C . Negative contours are dashed and zero contour is omitted. The H denotes the anticyclone perturbation location under study.

confirming the shallow character of the cold surge. Also, at lower and middle troposphere, the specific humidity perturbation exhibits a negative center (dry air) on the lee side with maximum magnitude between 850 and 900 hPa (Fig. 12c). Significant equatorward fluxes of negative moisture perturbations are also found on the lee side with a maximum at 850 hPa (Fig. 12d).

5. Summary and conclusions

By using an EEOF technique the most active synoptic-scale patterns over South America at 300 hPa during austral winter were identified. Two preferred propagation paths were identified: the track along the subpolar jet latitudes (EEOF 1 and EEOF 2) and that along subtropical jet latitudes (EEOF 3 and EEOF 4). This paper focuses on the systems evolving over subtropical South America, and given that EEOF 3 and EEOF 4 represent the evolution of the same wave pattern, the

latter is chosen because its phase is more favorable for the analysis.

The observed structure of the waves associated with the most active episodes of the subtropical mode features the typical characteristics of midlatitude baroclinic waves [already described by Lim and Wallace (1991) and Chang (1993) for the Northern Hemisphere, among others] like the maximum amplitude for both geopotential height and meridional wind perturbations at upper levels, the dynamical structure of cold lows and warm highs, the westward vertical tilt with height of geopotential height perturbations, and the eastward vertical tilt of temperature perturbations.

Perturbations exhibit significant modifications in their three-dimensional structure as they cross the Andes at middle latitudes from the South Pacific Ocean toward South America. The main wave structure changes are the following: 1) The lower-level perturbation advances following the shape of the Andes Mountains, and ex-

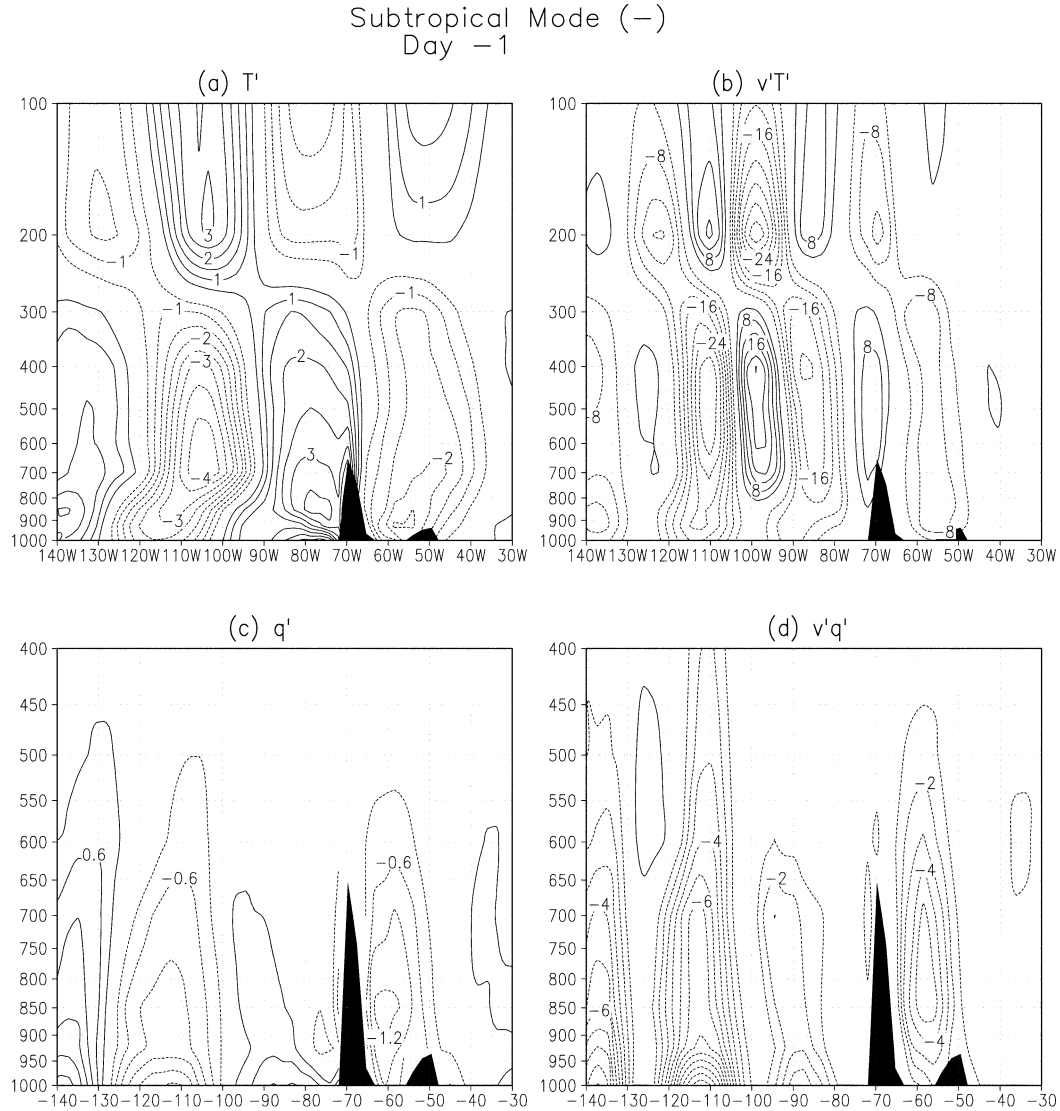


FIG. 12. Longitude–height cross section of negative composites for the subtropical mode of (a) temperature perturbations and (b) eddy meridional heat fluxes, averaged between 35° and 25° S at day -1 . Contour interval is (a) 0.35° C and (b) 3 m s^{-1} °C. Negative contours are dashed and zero contour is omitted. A sketch of the orography is included for reference.

periences an abrupt equatorward migration on the lee side of the mountains, as a result it becomes temporarily detached from the upper-level perturbation, which progresses eastward almost unaffected by the orography; and 2) the vertical structure of the temperature perturbation on the lee side of the mountains is modified in such a way that the maximum amplitude is near the surface and decreases with height. As a consequence, smaller eddy heat fluxes are found in the vicinity of the orography, contributing to a weaker eddy baroclinic growth there, in agreement with results by Bannon (1992) and Davis (1997) for the Rockies. Once the upper-level system is on the lee side, the perturbation turns to a more favorable baroclinic structure and thus low-level perturbation intensification occurs toward the east

of the continent. By that time, intense precipitation events are observed over southeastern South America, in association with enhanced moisture fluxes taking place along the eastern portion of the low-level cyclone. Over the ocean, the moisture maximum is at the surface, but over subtropical South America the moisture and moisture fluxes are largest around 850 hPa (see Figs. 8 and 11c,d). This suggests that local moisture changes are mainly controlled by advective processes, with the source of moisture located at the Tropics (with the caution that moisture analyses may be questionable over regions of sparse observations).

The analysis of the perturbation vorticity equation at 925 hPa showed that wind convergence near the surface is the main factor responsible for low-level cyclone

strengthening over southeastern South America. This low-level convergence is associated with an increment of the ascending motions at middle levels. Furthermore, through the analysis of the thermodynamic equation at 500 hPa, it was found that latent heat released by the precipitation events provide the main contribution to the upward motion enhancement at middle levels.

Finally, it was found that 60% of the cases within the composite correspond to offshore cyclone reinforcement, while the remaining 40% correspond to cyclone reinforcement over land. On average, the former are 25% deeper and the 24-h 1000-hPa height drop is 50% larger than in the latter. It is suggested that the presence of the warm waters of the Brazil Current seems to provide an additional source of moisture and heat that reduces static stability at low levels and thus contributes to cyclogenesis over the ocean. These results should be confirmed by future process studies on the nature of the air-sea interaction over the southwestern Atlantic.

Acknowledgments. Thanks are due to the reviewers that suggested changes to improve this manuscript. This article is partially funded by the Inter American Institute for Global Change Studies through the Cooperative Research Network Grant 055. The research of C. Vera and P. Vigliarolo was supported by UBA Grants JX80 and TW22, while E. H. Berberry's contribution was supported by NOAA Grant NA06GP0452 (PACS). ECMWF reanalyses were provided by CPTEC/INPE of Brazil through the LBA program. OLR datasets are available from the Climate Diagnostic Center (NOAA), and the Argentinean Weather Service provided the precipitation datasets.

REFERENCES

- Bannon, P. R., 1992: A model of Rocky Mountain lee cyclogenesis. *J. Atmos. Sci.*, **49**, 1510–1522.
- Berberry, E. H., and M. N. Nunez, 1987: Ciclogenesis al este de los Andes: Influencia dinamica de la cordillera en su desarrollo (Cyclogenesis east of the Andes: Dynamical influences during its development). *Proc. Second Int. American Conf. of Meteorology*, Buenos Aires, Argentina, Federacion Latinoamericana de Sociedades de Meteorologia, 21–27.
- , and C. S. Vera, 1996: Characteristics of the Southern Hemisphere winter storm track with filtered and unfiltered data. *J. Atmos. Sci.*, **53**, 468–481.
- , and E. A. Collini, 2000: Springtime precipitation and water vapor flux over southeastern South America. *Mon. Wea. Rev.*, **128**, 1328–1346.
- Blackmon, M. L., R. A. Madden, J. M. Wallace, and D. S. Gutzler, 1979: Geographical variations in the vertical structure of geopotential height fluctuations. *J. Atmos. Sci.*, **36**, 2450–2466.
- Buzzi, A., and E. Tosi, 1989: Statistical behavior of transient eddies near mountains and implications for theories of lee cyclogenesis. *J. Atmos. Sci.*, **46**, 1233–1249.
- Carrera, M. L., J. R. Gyakum, and D.-L. Zhang, 1999: A numerical case study of secondary marine cyclogenesis sensitivity to initial error and varying physical processes. *Mon. Wea. Rev.*, **127**, 641–660.
- Chang, E. K. M., 1993: Downstream development of baroclinic waves as inferred from regression analysis. *J. Atmos. Sci.*, **50**, 2038–2053.
- , 1999: Characteristics of wave packets in the upper troposphere. Part II: Seasonal and hemispheric variations. *J. Atmos. Sci.*, **56**, 1729–1747.
- Compagnucci, R. H., and M. A. Salles, 1997: Surface pressure patterns during the year over southern South America. *Int. J. Climatol.*, **17**, 635–653.
- Davis, C. A., 1997: The modification of baroclinic waves by the Rocky Mountains. *J. Atmos. Sci.*, **54**, 848–868.
- Gan, M. A., and V. B. Rao, 1991: Surface cyclogenesis over South America. *Mon. Wea. Rev.*, **119**, 1293–1302.
- , and —, 1994: The influence of the Andes Cordillera on transient disturbances. *Mon. Wea. Rev.*, **122**, 1141–1157.
- Garreaud, R. D., 2000: Cold air incursions over subtropical and tropical South America: Mean structure and dynamics. *Mon. Wea. Rev.*, **128**, 2544–2559.
- Hoskins, B. J., I. N. James, and G. H. White, 1983: The shape, propagation, and mean-flow interaction of large-scale weather systems. *J. Atmos. Sci.*, **40**, 1592–1612.
- Hsu, H.-H., 1987: Propagation of low-level circulation features in the vicinity of mountain ranges. *Mon. Wea. Rev.*, **115**, 1864–1892.
- , and J. M. Wallace, 1985: Vertical structure of wintertime teleconnection patterns. *J. Atmos. Sci.*, **42**, 1693–1710.
- Jusem, J. C., and R. Atlas, 1991: Diagnostic evaluation of numerical model simulations using the tendency equation. *Mon. Wea. Rev.*, **119**, 2936–2955.
- Lau, K.-H., and N.-C. Lau, 1990: Observed structure and propagation characteristics of tropical summertime synoptic-scale disturbances. *Mon. Wea. Rev.*, **118**, 1888–1913.
- Lau, K.-M., and P. Chan, 1985: Aspects of the 40–50 day oscillation during the northern winter as inferred from outgoing longwave radiation. *Mon. Wea. Rev.*, **113**, 1889–1909.
- Lim, G. H., and J. M. Wallace, 1991: Structure and evolution of baroclinic waves as inferred from regression analysis. *J. Atmos. Sci.*, **48**, 1718–1732.
- Mak, M., 1998: Influence of surface sensible heat flux on incipient marine cyclogenesis. *J. Atmos. Sci.*, **55**, 820–834.
- Marengo, J., A. Cornejo, P. Satyamurti, C. Nobre, and W. Sea, 1997: Cold surges in tropical and extratropical South America: The strong event in June 1994. *Mon. Wea. Rev.*, **125**, 2759–2786.
- Necco, G. V., 1982a: Comportamiento de vórtices ciclónicos en el área sudamericana durante el FGGE: Ciclogénesis (Behavior of the cyclonic vortices in the South American region during FGGE: Cyclogenesis). *Meteorologica*, **13**, 7–20.
- , 1982b: Comportamiento de vórtices ciclónicos en el área sudamericana durante el FGGE: Trayectorias y desarrollos (Behavior of the cyclonic vortices in the South American region during FGGE: Tracks and developments). *Meteorologica*, **13**, 21–34.
- Peterson, R. G., and L. Stramma, 1991: Upper-level circulation in the South Atlantic Ocean. *Progress in Oceanography*, Vol. 26, Pergamon Press, 1–73.
- Saraiva, J. M. B., and P. L. Silva Dias, 1997: A case study of intense cyclogenesis off the southern coast of Brazil: Impact of SST, stratiform and deep convection. Preprints, *Fifth Conf. on Southern Hemisphere Meteorology and Oceanography*, Pretoria, South Africa, Amer. Meteor. Soc., 368–369.
- Seluchi, M. E., and A. C. Saulo, 1997: Simulación de 10 episodios de ciclogénesis costeras sobre Sudamérica utilizando un modelo regional (Simulation of 10 episodes of coastal cyclogenesis over South America using a regional model). *Meteorologica*, **22**, 49–66.
- , and —, 1998: Possible mechanisms yielding an explosive coastal cyclogenesis over South America: Experiments using a limited area model. *Aust. Meteor. Mag.*, **47**, 309–320.
- , Y. V. Serafini, and H. Le Treut, 1998: The impact of the Andes on transient atmospheric systems: A comparison between observations and GCM results. *Mon. Wea. Rev.*, **126**, 895–912.
- Simmonds, I., and K. Keay, 2000: Mean Southern Hemisphere extratropical cyclone behavior in the 40-Year NCEP–NCAR Reanalysis. *J. Climate*, **13**, 873–885.
- Taljaard, J. J., 1972: Synoptic meteorology in the Southern Hemis-

- sphere. *Meteorology of the Southern Hemisphere*, Meteor. Monogr., No. 35, Amer. Meteor. Soc., 139–213.
- Trenberth, K. E., 1981: Observed Southern Hemisphere eddy statistics at 500 mb: Frequency and spatial dependence. *J. Atmos. Sci.*, **38**, 2585–2605.
- Uccellini, L. W., 1990: Processes contributing to the rapid development of extratropical cyclones. *Extratropical Cyclones: The Erik Palmén Memorial Volume*, C. W. Newton and E. O. Holopainen, Eds., Amer. Meteor. Soc., 81–105.
- Vera, C. S., and P. K. Vigliarolo, 2000: A diagnostic study of cold-air outbreaks over South America. *Mon. Wea. Rev.*, **128**, 3–24.
- Vigliarolo, P. K., C. S. Vera, and S. Diaz, 2001: Southern Hemisphere winter ozone fluctuations. *Quart. J. Roy. Meteor. Soc.*, **127**, 559–578.
- Walsh, C. H., J. E. Peak, W. F. Calland, and W. A. Cook, 1988: Diagnostic study of explosive cyclogenesis during FGGE. *Mon. Wea. Rev.*, **116**, 431–451.
- Weare, B. C., and J. S. Nasstrom, 1982: Examples of extended empirical orthogonal function analyses. *Mon. Wea. Rev.*, **110**, 481–485.
- Xie, P., and P. A. Arkin, 1997: Global precipitation: A 17-year monthly analysis based on gauge observations, satellite estimates, and numerical model outputs. *Bull. Amer. Meteor. Soc.*, **78**, 2539–2558.
- Yu, J.-Y., and D. L. Hartmann, 1995: Orographic influences on the distribution and generation of atmospheric variability in a GCM. *J. Atmos. Sci.*, **52**, 2428–2443.